

See discussions, stats, and author profiles for this publication at: <https://www.researchgate.net/publication/51189499>

Chemometric Labeling of Cereal Tissues in Multichannel Fluorescence Microscopy Images Using Discriminant Analysis

ARTICLE *in* ANALYTICAL CHEMISTRY · NOVEMBER 1997

Impact Factor: 5.64 · DOI: 10.1021/ac970145x · Source: PubMed

CITATIONS

14

READS

50

6 AUTHORS, INCLUDING:



Dominique Bertrand

data_frame

190 PUBLICATIONS 2,504 CITATIONS

SEE PROFILE

Chemometric Labeling of Cereal Tissues in Multichannel Fluorescence Microscopy Images Using Discriminant Analysis

Paul M. Baldwin, Dominique Bertrand, Bruno Novales, Brigitte Bouchet, Gaëlle Collobert, and Daniel J. Gallant*

Laboratoire de Technologie Appliquée à la Nutrition, Institut National de la Recherche Agronomique (INRA), Centre de Recherche de Nantes, 44316 Nantes Cedex 03, France

This paper presents a novel, semiautomatic method for microscopic identification of multicomponent samples, which allows the identification, location, and percentage quantity of each component to be determined. The method involves applying discriminant analysis to a sequence of multichannel fluorescence microscopy images via a supervised learning approach; by selecting groups of pixels that are representative for each component type in a “known” sample, a computer is “taught” how to recognize the behavior (i.e., fluorescence emission) of the various components when illuminated under different spectral conditions. The identity, quantity, and location of these components in “unknown” samples (i.e., samples with the same component types but in different ratios or distributions) can then be investigated. The technique therefore enables semiautomatic quantitative fluorescence microscopy and has potential as a quality control tool. This work demonstrates the application of the technique to artificial and natural samples and critically discusses its quality, potential, and limitations.

In many microscopic studies, identification and discrimination between different biological or histochemical structures within complex, multicomponent samples is desired.¹ Such samples exist in practically all domains of science where two or more compounds exist together, e.g., creams, paper, living cells, and most food systems. The cereal grain serves as a natural example of a multicomponent sample, since it contains a variety of different tissues, e.g., bran (pericarp, tegument, seminal tegument, aleurone cells), endosperm, and germ.^{2–4} The bran and germ remaining in the flour after cereal processing are technically termed “contaminants”, although they are often viewed as beneficial in terms of providing dietary fiber and minerals.^{5,6} Furthermore, it is their relative quantities, in association with flour color and

protein content, that largely determine the quality of flour and thus dictate its end usage.^{6–8}

Both spatial and nonspatial techniques have been used for identifying the components of cereal products for quality control during processing. While the nonspatial techniques (e.g., mid- and near-infrared spectroscopy and fluorescence spectroscopy) have found some use for quantitative assessment of bulk biochemical composition,^{9–11} such techniques cannot currently characterize the detailed local organization of the samples. Spatial techniques (macroscopy and microscopy) on the other hand offer the advantage of detailed characterization of the heterogeneity and spatial organization of complex products.^{12,13} This is commonly (and most simply) performed using specific dyes to mark the various components, allowing visual identification.¹⁴ Fluorescence microscopy is particularly attractive for this task^{15–17} since it is highly sensitive and provides spatial localization of the sample with high optical resolution at the microscopic scale. The spectral conditions of fluorescence (which occurs when a portion of light absorbed by a substance is re-emitted in the form of longer wavelength radiation) are defined by a pair of wavelengths: the *excitation wavelength* (λ_{exc}), and the *emission wavelength* (λ_{em}).¹⁸ Fluorescence microscopy makes use of both highly chemically specific fluorochrome dyes and naturally occurring autofluorescent compounds, e.g., lignin, and the phenolic compounds found in aleurone cell walls,¹⁹ and is thus increasingly being used for determination of cereal product quality^{5,20–22} and in food product quality evaluation in general.^{15,23}

- (1) Munck, L., Ed. *Fluorescence Analysis in Foods*; Longman Scientific and Technical: Harlow, UK, 1989; pp 1–32.
(2) MacMasters, M. M.; Hinton, J. J. C.; Bradbury, D. *Wheat: Chemistry and Technology*; American Association of Cereal Chemists: St. Paul, MN, 1978; pp 51–113.
(3) Fincher, G. B.; Stone, B. A. *Adv. Cereal Sci. Technol.* **1986**, 8, 207–295.
(4) Jenner, C. F.; Ugalde, T. D.; Aspinall, D. *Aust. J. Plant. Physiol.* **1991**, 18, 211–226.
(5) Munck, L.; Feil, C. In *Cereals for food and beverages: Recent progress in chemistry and technology*; Inglett, G. E., Munck, L., Eds.; Academic Press: New York, 1980; pp 27–40.
(6) Saunders, R. M. In *Cereals for food and beverages: Recent progress in chemistry and technology*; Inglett, G. E., Munck, L., Eds.; Academic Press: New York, 1980; pp 137–153.
(7) Wall, J. S. In *Recent Advances in the Biochemistry of Cereals*; Laidman, D. L., Wyn Jones, R. G., Eds.; Academic Press: London, UK, 1979; pp 275–311.
(8) Branlard, G.; Dardevet, M. *J. Cereal Sci.* **1985**, 3, 345–354.
(9) Williams, P. C.; Thompson, B. N.; Wetzel, D.; McLay, G. W.; Loewen, D. *Cereal Foods World* **1981**, 26, 234–237.
(10) Osbourne, B. G.; Douglas, S.; Fearn, T. *J. Food Technol.* **1982**, 17, 355–363.
(11) Robert, P.; Bertrand, D.; Devaux, M.-F. *Sci. Aliments* **1988**, 8, 113–131.
(12) Pussayanawin, V.; Wetzel, D. L.; Fulcher, R. G. *J. Agric. Food Chem.* **1988**, 36, 515–520.
(13) Irving, D. W.; Fulcher, R. G.; Bean, M. M.; Saunders, R. M. *Cereal Chem.* **1989**, 66, 471–477.
(14) Clark, G. *Staining Procedures*, 4th ed.; Williams & Wilkins: Baltimore, MD, 1981.
(15) Fulcher, R. G.; Irving, D. W.; de Francisco, A. *Fluorescence Analysis in Foods*; Longman Scientific and Technical: Harlow, UK, 1989; pp 59–109.
(16) Gallant, D. J.; Irving, D. W. *Anal. Mag.* **1991**, 19, M25–M31.
(17) Irving, D. W.; Gallant, D. J. *Microsc. Anal.* **1993**, (March), 15–17.
(18) Guilbault, G. G. *Fluorescence Analysis in Foods*; Longman Scientific and Technical: Harlow, UK, 1989; pp 31–58.
(19) Fulcher, R. G.; O'Brien, T. P.; Lee, J. W. *Aust. J. Biol. Sci.* **1972**, 25, 23–34.

Fluorescence microscopy is ideally coupled with an artificial vision system, allowing the acquisition and subsequent manipulation of numeric (digital) images of the sample. Artificial vision and image analysis^{21,24–26} is finding increasing quality control applications in the food industry, due to its flexibility, repeatability and low cost.²⁶ Quality control of cereal products using macroscopic artificial vision has been extensively studied and can be used for the discrimination of cereal types by the appearance of their kernels^{27–29} and the detection of foreign materials.^{27,30} Considerable effort has also been directed at achieving microscopic quantification of endosperm, aleurone, and pericarp in wheat milling fractions in order to predict flour quality^{13,22} and in relating such quantification to the ash or ferulic acid content of the flours.^{12,31} The exact fluorescence intensity emitted from a compound is dependent, however, on a range of external and environmental factors including physical sample thickness, sample viscosity, illumination stability with time, temperature, pH, quenching, and bleaching.¹⁸ Quantitative measurement of fluorophore concentrations by virtue of their emitted fluorescence intensity is therefore notoriously problematic, requiring awareness and (where possible) control of all the factors influencing the intensity of fluorescence emission from the sample, in addition to the use of stable fluorescence standards which are often expensive. A commercial fluorescence microscopy device, the DIPIX I440 system,³² has however been marketed; it exploits the autofluorescence of cereal tissues to achieve automatic determination of cell wall contamination in cereal flours. In this system, the gray level histograms of many fields of view are processed in order to calculate the percentage of the total surface area viewed that is aleurone or pericarp. The system does not therefore offer the possibility of studying the spatial distribution of such multicomponent samples.

However, by acquiring a digital image sequence of a multicomponent sample in which each image is taken under different spectral conditions (λ_{exc} and λ_{em}), it is often possible (either with autofluorescence or by addition of fluorochromes) to find spectral conditions under which each individual component in the sample exhibits a unique fluorescence behavior. Each digital image in the sequence can be regarded as a 2D table of numbers (i.e., pixels), where each number is a measure of the light intensity emitted from the corresponding area of the sample (and is called the *gray level value* of the pixel). Each number in the table thus has unique *x,y* coordinates, and its gray level value will fall between 0 and a fixed upper number (e.g., 255 when an 8-bit integer is used by the computer to store the pixel gray level values). The gray level values (called the *gray scale*) thus range from 0 to 255 (i.e., 2^{10} to 2^8 -1).

- (20) Fulcher, R. G.; Faubion, J. M.; Ruan, R.; Miller, S. S. *Carbohydr. Polym.* **1994**, *25*, 285–293.
- (21) Harrigan, K. *Cereal Foods World* **1995**, *40*, 11–14.
- (22) Symons, S. J.; Dexter, J. E. *J. Cereal Sci.* **1996**, *23*, 73–83.
- (23) Fulcher, R. G.; Wood, P. J.; Yiu, S. H. *Food Technol.* **1984**, *38*, 101–106.
- (24) Bertrand, D.; Devaux, M.-F.; Robert, P. *Trends Anal. Chem.* **1991**, *10*, 237–243.
- (25) Gonzalez, R. C.; Shapiro, L. G. *Digital Image Processing*; Addison-Wesley Publishing Co.: Reading, MA, 1992.
- (26) Gunasekaran, S. *Trends Food Sci. Technol.* **1996**, *7*, 245–256.
- (27) Zayas, I.; Lai, F. S.; Pomeranz, Y. *Cereal Chem.* **1986**, *63*, 52–56.
- (28) Sapirstein, H.; Neuman, M.; Wright, E. H.; Shwedyk, E.; Bushuk, W. *J. Cereal Sci.* **1987**, *6*, 3–14.
- (29) Chen, C.; Chiang, Y. P.; Pomeranz, Y. *Cereal Chem.* **1989**, *66*, 466–470.
- (30) Zayas, I.; Pomeranz, Y.; Lai, F. S. *Cereal Chem.* **1989**, *66*, 233–237.
- (31) Symons, S. J.; Dexter, J. E. *Cereal Chem.* **1991**, *68*, 454–460.
- (32) Scott, A. J.; Ching Yang, W. T. *Anal. Mag.*, **1991**, *19*, 31–34.

The sequence of digital images is termed a “multichannel image” and is in effect a multitable data storage space of *z* two-dimensional arrays of numbers (gray level values), where *z* represents the number of different spectral conditions. Assuming that the multichannel image contains at least one image for each component which shows its unique fluorescence behavior, there is sufficient data to allow all of the components to be distinguished. However, since it is possible to have many spectral conditions (defined by the pair of excitation and emission wavelengths) it is evident that extensive multitable data can be generated, e.g., a sequence of six 512×512 pixel images has 1 572 864 pixels. Thus, in order to efficiently access and process the data contained in multichannel images, it is necessary to develop and apply chemometric mathematical approaches adapted to the rapid analysis of extensive multitable data. Stepwise discriminant analysis (SDA)^{33–35} is suited to this purpose. SDA is a “supervised learning” method in which a procedure for classifying data into qualitative groups is developed following a training stage where the characteristics that discriminate between sets of representative data with “known” differences are selected. The technique has previously been adapted to the analysis of multichannel images by the authors and has allowed the development of a near-infrared spectral imaging system^{36,37} and a macroscopic fluorescence imaging system.³⁸

This paper presents the novel application of stepwise discriminant analysis to multichannel fluorescence microscopy images, creating a powerful new analytical technique for the direct identification and spatial visualization of multicomponent samples at the microscopic scale. Single labeled images are created from multichannel image sequences in which each component in the sample is displayed with a separate false color, thus allowing it to be identified, located, and quantified. Initially, the quality of image labeling was tested using a “control” multicomponent sample (fluorochrome-labeled latex beads of different sizes). Discriminant labeling of the various tissues in a wheat grain section was then performed as an illustrative example of the potential of this technique.

MATERIAL AND METHODS

Samples and Sample Preparation. **1. Fluorescent Latex Beads.** Fluorophore-labeled latex beads of three different sizes (nominally 15, 10, and 4 μm diameters) were purchased. The 15 and 10 μm diameter beads (Fluospheres, Molecular Probes Europe BV, Leiden, The Netherlands) had particle sizes (diameters) of $15.5 \mu\text{m} \pm 2.1\%$ and $9.7 \mu\text{m} \pm 1.0\%$, respectively (Certificate of Analysis, Molecular Probes). The 15 μm diameter beads were red fluorescent (λ_{exc} 580 nm/ λ_{em} 605 nm). The 10 μm diameter beads were orange fluorescent (λ_{exc} 530 nm/ λ_{em} 560 nm). Both the 15 and 10 μm diameter beads were supplied sterile, suspended in distilled water with 0.02% Tween-20 and 0.9% NaCl,

- (33) Romeder, J. M. *Méthodes et Programmes d'Analyse Discriminante*; Bordas: Paris, France, 1973.
- (34) Sharaf, M. A.; Illman, D. L.; Kowalski, B. R. *Chemometrics*; John Wiley & Sons: New York, 1986.
- (35) Bertrand, D.; Courcoux, P.; Autran, J.-C.; Meritan, R.; Robert, P. *J. Chemom.* **1990**, *4*, 413–427.
- (36) Robert, P.; Bertrand, D.; Devaux, M.-F.; Sire, A. *Anal. Chem.* **1992**, *64*, 664–667.
- (37) Bertrand, D.; Robert, P.; Novales, B.; Devaux, M.-F. *Proceedings of 7th International Conference on Near Infrared Spectroscopy*; NIR Publications: Montréal, Canada, 1996; pp 174–178.
- (38) Novales, B.; Bertrand, D.; Devaux, M.-F.; Robert, P.; Sire, A. *J. Sci. Food Agric.* **1996**, *71*, 376–382.

(0.2% solids with, respectively, 9.8×10^5 and 3.99×10^6 particles/mL). The 4 μm diameter beads (Cheminex SA, Maisons Alfort, France) were green fluorescent (λ_{exc} 488 nm/ λ_{em} 515–520 nm) and were supplied in a phosphate buffered saline (PBS) suspension with 0.01% azide (7.0×10^4 particles/mL).

A 1 mL sample of each latex bead was mixed and a drop of the mixture deposited on a microscope slide to create a “control” well-characterized multicomponent sample, in which each component possessed different fluorescence characteristics and could also be identified according to its particle size in order to verify correct labeling.

2. Cereal Samples. Whole wheat grains (variety *Falcon*; INRA, Nantes, France) were placed onto moistened filter paper for ~ 4 h (to allow samples to become damp). Samples were then rapidly frozen to -20°C in a microtome–cryostat (HM500 OM, Microm, Francheville, France) and cut into 10 μm thick sections. Sections were directly mounted onto optical microscope slides, with nonfluorescent mounting oil and a cover slip.

Fluorescence Microscopy and Image Acquisition. An epifluorescence optical microscope (Leica, Model DMRB) with three light sources (a standard 12 V halogen bright-field lamp, a 50 W high-pressure mercury vapor lamp, and a 75 W xenon lamp) was used. The mercury lamp presented a discontinuous illumination spectrum with specific sharp peaks, whereas the spectrum of the xenon lamp displayed more uniform intensity from 400 to 800 nm. The microscope was equipped with four filter blocks (coded A–D), making it possible to select four excitation/emission wavelengths; filter block A excitation at 530–595 nm, emission >615 nm; B excitation at 516–560 nm, emission >580 nm; C excitation at 450–490 nm, emission >520 nm; D excitation at 340–380 nm, emission >430 nm. By combining one of the two light sources (Hg or Xe) and one of the four filter blocks, it was possible to obtain up to eight different fluorescence spectral conditions. Observation of the sample under bright-field conditions provided a ninth spectral condition.

The microscope was fitted with a sensitive cooled CCD camera (Model CH 250; Photometrics Ltd., Tucson, AZ; sensitivity, 1×10^{-5} lux) which allowed the acquisition of 512×512 pixel images, the gray levels of which were coded on 12 bits (from 0 to 4095). Sequences of up to nine images were therefore acquired for each sample investigated, with one image for each spectral condition. The magnification of the microscope (40 \times or 20 \times) in association with the camera imaging optics resulted in an image representing (respectively) either a 180×180 or $90 \times 90 \mu\text{m}^2$ area of the object.

Mathematical Procedures for Labeling Images. By varying the spectral conditions, a multichannel image of the sample was acquired, with each image in the series containing different fluorescence information. The sample was therefore characterized by a sequence of images, which can be represented by a three-dimensional table P . Each element in this table, $P_{x,y,z}$, corresponds to the gray level value at the position (x,y) under the spectral condition z. A pixel $P_{x,y}$ can therefore be represented by a vector, which has z points, with the points sequentially having values representative of the gray level value of the pixel at each spectral condition.

In order to extract the discriminant data from these pixel vectors, it was necessary to develop methods by which a computer could “recognize” the characteristic behavior of a pixel belonging to each of the components in the sample. This learning process was achieved using supervised stepwise discriminant analysis.^{33–35}

Stepwise Discriminant Analysis. In SDA of multichannel images, it is assumed that the user is able to select sets of pixels (collectively termed the “learning set”), which are representative of the various components in the sample. In the present study, between 150 and 300 representative pixels were manually selected for each group, using macros written by the authors with the PMIS image processing software supplied with the Photometrics CCD camera. The gray level value of each selected pixel, in *each* image of the sequence, was extracted and recorded in an ASCII data file, along with the x,y coordinates of the pixel. Furthermore, each representative pixel (including pixels from the image background) was given a unique qualitative *group number* which corresponded to the component for which it was representative. Thus, in a multichannel image sequence containing nine images, the data extracted for each representative pixel would include its qualitative group, its x,y location in the image, and the nine different gray level values constituting its pixel vector.

The next process was to apply stepwise discriminant analysis on this “learning set” of representative pixel vectors in order to find “structures” or “patterns” in the data that are discriminant for each component of the sample. The process of SDA has been extensively described by Bertrand et al.³⁷ and was performed using programs written by the authors in the C language. In brief, SDA initially involves data reduction by selection of the minimum number of spectral conditions that provide the most discrimination between the components in the sample (i.e., redundant data are eliminated, and the pixel vector is shortened). This is achieved by assessing the percentage of correct pixel group classification given by each spectral condition. Initially, each spectral condition is treated separately. Average gray level intensity values are found for each qualitative group. If the spectral condition contains useful discriminant information these average gray level intensity values should be significantly different from one another. The percentage of correct pixel group classification given by a spectral condition is then calculated by “comparing” the gray level value of each pixel in the learning set with the average gray level intensity values for the various groups. Each pixel is attributed to the group whose average intensity value is the most similar to the pixel’s intensity value. Once all the pixels in the learning set have been attributed to a group, the percentage of correct classification is calculated, using the knowledge of the real qualitative groups as originally designated by the operator. The “comparisons” were performed via application of a Mahalanobis metric distance calculation,³⁹ the formula for which is shown below,

$$d_{A,B} = [(\mathbf{a} - \mathbf{b})^T \cdot \text{Cov}^{-1} (\mathbf{a} - \mathbf{b})]^{1/2}$$

where $d_{A,B}$ is the Mahalanobis metric distance between the two data points A and B, \mathbf{a} and \mathbf{b} are the pattern vectors associated with the points A and B, T denotes the transformed vector, and Cov is the full variance–covariance matrix for the original data.

The Mahalanobis metric distance is thus a positive number, which is small when the value of the data point (e.g., A) is similar to the average value (or *center of gravity*) of the data points of a certain group (e.g., B) and large when the value of the data point is substantially different from the average value of the data points

(39) Adams, M. J. *Chemometrics in Analytical Spectroscopy*; The Royal Society of Chemistry: Cambridge, UK, 1995.

of a certain group. Consequently, in the simple case where we consider just one spectral condition at a time, if the gray level value of a given pixel under a given spectral condition has the smallest value of the Mahalanobis metric distance when compared to the value of the center of gravity for, say, group 2, (as opposed to its Mahalanobis metric distance to the center of gravity of the other groups) this pixel is predicted to belong to group 2.

Once the percentage of correct classification provided by each individual spectral condition has been calculated, the condition providing the highest correct classification is kept as a starting *discrimination model*, and the other conditions (in decreasing order of their prediction ability) are sequentially added (hence the term "stepwise") to the model. The ability to correctly classify all of the pixels in the learning set is tested at each step via application of the Mahalanobis metric distance calculation (with the addition of spectral conditions increasingly lengthening the pixel vector and increasing the "*dimensions*" in the discrimination model). A step is thus found in which maximal discrimination is achieved which, in general, does not require the use of all of the spectral conditions. Data from unrequired spectral conditions are then rejected, and the remaining data are then gathered into a matrix \mathbf{X} , in which the rows represent the pixels and the columns represent the remaining (usefully discriminant) spectral conditions. A given value in this matrix, x_{ij} , thus represents the gray level value of the pixel i , with the spectral condition numbered j .

The next step is to map these remaining gray level intensity values into an imaginary *multidimensional* space, where the number of *dimensions* is equal to the number of retained spectral conditions. This is again achieved using the Mahalanobis metric distance, such that each qualitative group is summarized by the average vector (or *center of gravity*) of the remaining gray level values of the representative pixels of this group. Assuming that good discrimination between the representative pixels from the various sample components has been achieved (via good selection of the spectral conditions), the centers of gravity for each group (i.e., for each sample component) should be well separated from one another in the multidimensional space. Furthermore, the individual pixel vectors of the representative pixels of each qualitative group should form discrete "clouds" or "clusters" of "points" around the center of gravity for that group. This imaginary multidimensional space with the centers of gravity for each qualitative group produces a *multidimensional discriminant model* (or *learning template*).

Next the shortened pixel vector of each pixel in the original multichannel image is mapped onto the learning template. Thus, let \mathbf{x} be the shortened pixel vector for one of the pixels to be classified, and let us suppose that there are k qualitative groups in our discriminant model. We thus assess k Mahalanobis metric distances, $d(\mathbf{g}_i, \mathbf{x})$ between each gravity center \mathbf{g}_i and \mathbf{x} , and attribute the observation \mathbf{x} to the group giving the smallest value of the distance. By performing this process for each pixel in the image, qualitative groups are attributed to every pixel in the image, thus creating a "labeled image". An arbitrary false color is attributed to each qualitative group, and the labeled image can then be displayed, showing the location of each component in the sample.

After this learning process has been performed once, the same discriminant learning template can be applied on any "unknown" multichannel image in order to predict the qualitative nature of each pixel and create further labeled images. An "unknown"

multichannel image means a multichannel image taken with the same spectral conditions as the learning image, but with a different area of the sample or with a new sample containing the same components as the original sample, but in different relative quantities.

RESULTS: ILLUSTRATIVE EXAMPLES

Artificial Samples. Fluorochrome-Labeled Latex Beads.

Artificial samples were initially studied in order to test the feasibility of the technique and to develop the procedures involved in labeling. Panels 1–6 of Figure 1 show a sequence of six images demonstrating that the three types of bead presented different fluorescence signatures when observed using a range of spectral conditions (block A, Xe; B, Xe; C, Xe; C, Hg; D, Xe; D, Hg). For example, in the first image (1_1) ($\lambda_{\text{exc}} = 530$ to 595 nm, $\lambda_{\text{em}} = >615$ nm, Xe lamp) the large ($15 \mu\text{m}$) beads were highly fluorescent (l), the medium ($10 \mu\text{m}$) beads displayed weak fluorescence (m) and the small ($4 \mu\text{m}$) beads (s) did not display a significant fluorescence (and are not visible). In the third image, however ($\lambda_{\text{exc}} = 450$ to 490 nm, $\lambda_{\text{em}} = >520$ nm, Xe lamp), the large beads displayed less intense fluorescence than the medium beads, while the small beads emitted a stronger fluorescence than previously.

The image sequence demonstrates that within a population of beads of the same size considerable variation in the intensity of fluorescence under any given spectral condition was possible. This is evident by comparing the fluorescence intensity of the right-hand large bead in image 3 with the fluorescence intensity of the other large beads. It is seen that in image 3 the right-hand large bead appears to behave more like a medium-sized bead. Observation of the sequence as a whole reveals, however, that, while variations exist, the spectral characteristics (i.e., the shape of the pixel vector) for each bead type is generally the same. These general pixel vector shapes are shown in Figure 2, where the mean spectral characteristics of pixels from the three different bead types and those of the background are displayed. The graph clearly shows the difference in the spectral signatures of each of the four groups.

In order to make use of these different spectral signatures, sets of representative pixels were selected for each component (300 pixels for the background, 150 for the small beads, 300 for the medium beads, and 250 for the large beads; 1000 pixels total) and stepwise discriminant analysis applied as detailed above. The percentage of correctly classified pixels calculated at each step for the images in panels 1–6 of Figure 1 is shown in Table 1. The best result (i.e., the highest correct classification of the pixels using the least number of spectral conditions) was achieved in step 4, where 995 out of 1000 pixels (i.e., 99.5%) were correctly classified using four out of the six images. The five incorrectly classed pixels were pixels of the large beads which were confused with pixels of the background.

Surprisingly, spectral condition five ($\lambda_{\text{exc}} = 340$ – 380 nm, $\lambda_{\text{em}} = >430$ nm, Xe lamp), under which all four components exhibited low intensities of fluorescence, was selected by the SDA as the most discriminating condition. This demonstrates that there is no obvious relationship between fluorescence intensity and discriminating ability (i.e., by using Mahalanobis distances, each spectral condition is given an equal chance to be discriminant irrespective of the actual intensity values). It is also interesting to note that, with only two images (panels 1 and 5), it was possible to obtain correct classification of nearly 95% of the learning pixels. It is therefore both valid and useful to show the "biplot" of the

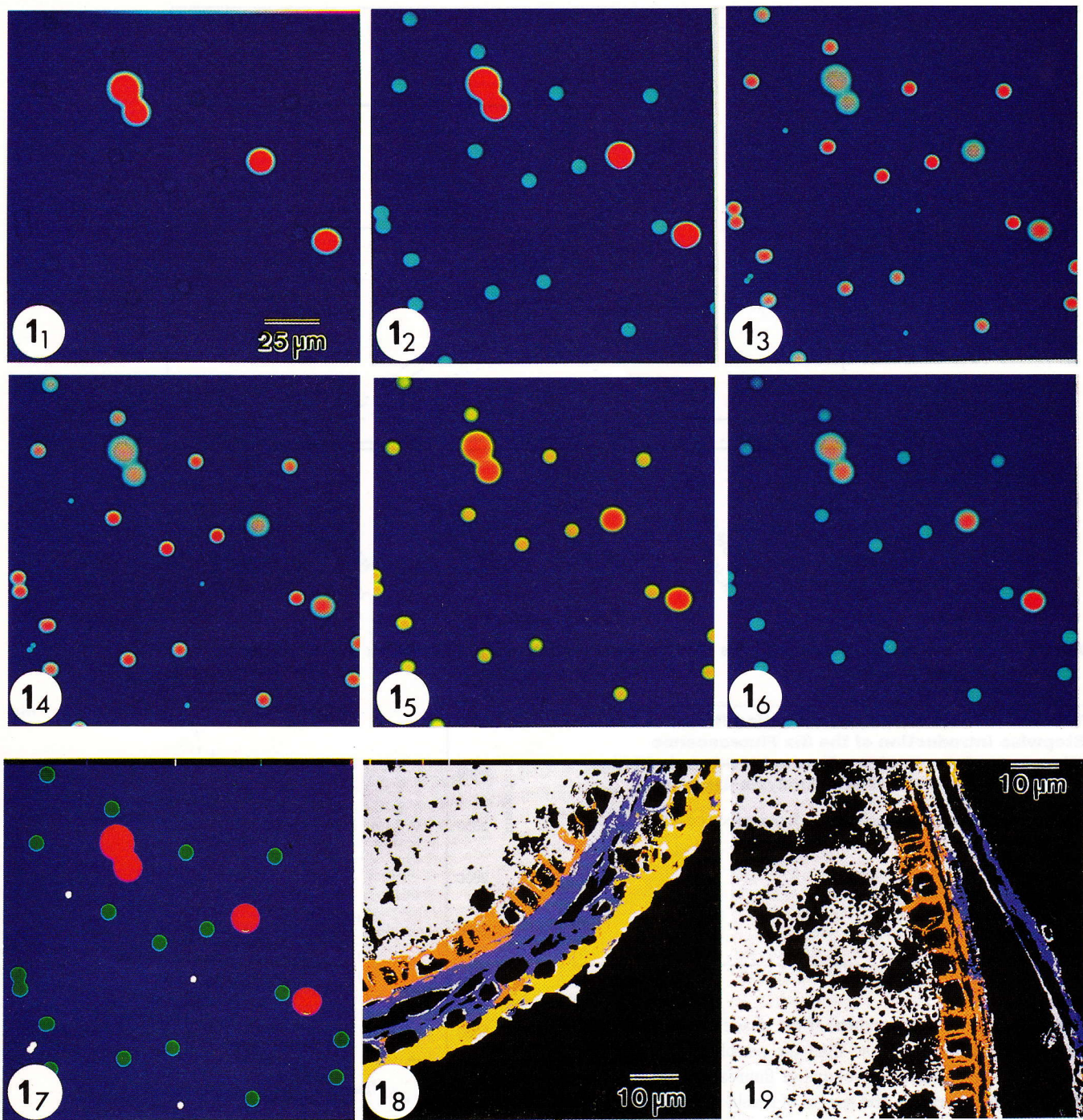


Figure 1. (Panels 1–6) Sequence of six fluorescence microscopy images showing the fluorescence emission of the fluorophore-labeled latex beads under varying spectral conditions. See Figure 2 for details of the spectral conditions. (Panel 7) Labeled image of the latex beads created from the learning procedure. Each group is labeled by a single gray level value which has an arbitrary false color (shown by the color bar). (Panel 8) Labeled image of the wheat grain section created from the learning procedure. Each group is labeled by a single gray level value which has an arbitrary false color (shown by the color bar). (Panel 9) An example of a “unknown” labeled image created using the discriminant “template” for the wheat section sample. The false color scale is the same as panel 8.

gray level values of these two images (Figure 3). A biplot is a 2D graphical representation of the discrimination achieved using two of the available parameters which are displayed on the *x* and *y* axes. The two parameters chosen are normally the two most discriminant parameters (e.g., spectral conditions in this case). Each pixel is coded by the first letter of the name of the group (b, background; s, small bead; m, medium bead; l, large bead). The mean pixel value of each group is represented by an uppercase large letter. For the sake of clarity, only nonoverlapping data points are shown, but this does not change the overall

interpretation of the graph. The pixels are generally well separated as a function of their qualitative group. Since only nonoverlapping pixels are shown, however, the graph gives no direct information on the local density of the points. Such information can be found by examining the position of the mean pixel value. For example the group of large beads (l) has some pixels that are spread in the direction of the background, but the location of the mean pixel value is far from the background mean value due to the high density of pixels at the top right area of the biplot. The spread of the large and medium pixel values is directly

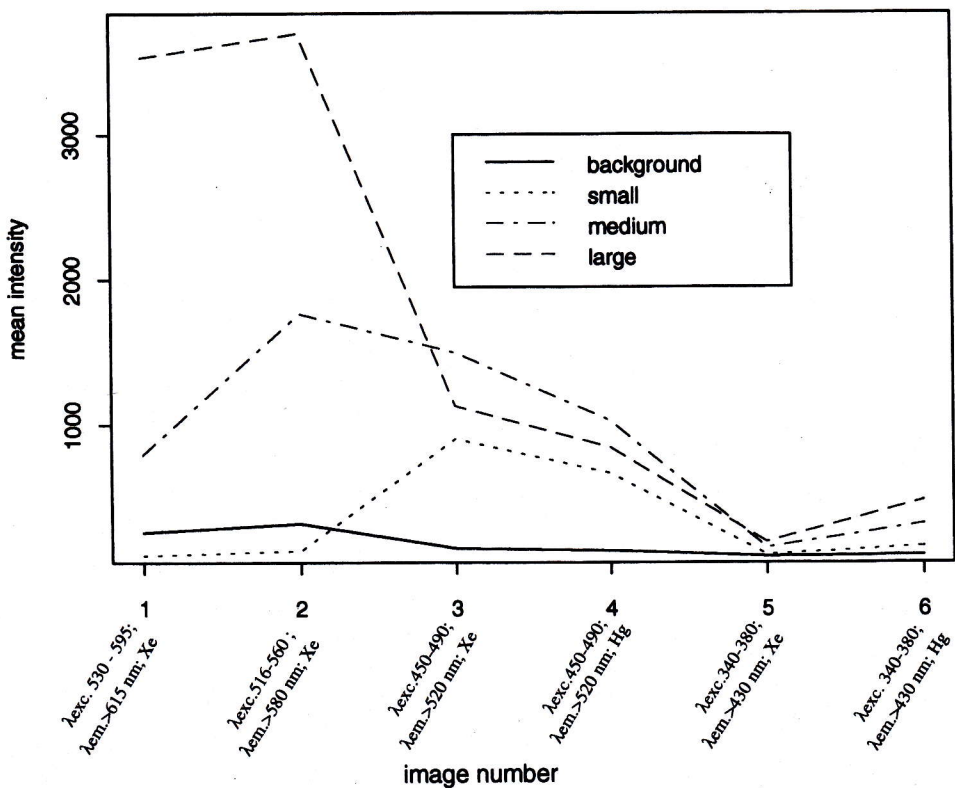


Figure 2. Spectral characteristics of the three bead types and the background under the six spectral conditions.

Table 1. Effects on the Classification Result of the Stepwise Introduction of the Six Fluorescence Microscopy Images of the Fluorophore-Labeled Latex Beads into the Discriminant Analysis Algorithm

step no.	no. of images included	% of correctly classified pixels
1	5	86.6
2	5; 1	94.4
3	5; 1; 2	98.4
4	5; 1; 2; 3	99.5
5	5; 1; 2; 3; 6	99.5
6	5; 1; 2; 3; 6; 4	99.5

caused by the spherical nature of the shape of the beads: the central part is more intense than the periphery, because it is representative of a greater volume of fluorescing material than the edge. Furthermore, the spread of pixels from all three bead types toward the background values results from the deliberate and necessary inclusion of representative pixels in each bead set which were located at the edge of the bead close to the background. In this way, during the learning stage (i.e., selection of representative pixels), the user sets the limits of the bead sizes. It is evident, however, that the intensity of the background is influenced by the close presence of the fluorescent spheres (hence the reciprocal spread of a small proportion of the background pixels toward the mean pixel value of each of the beads).

Following the learning stage, the discriminating model obtained from the SDA was applied to all of the pixels (as explained above) creating a single labeled image. An example labeled image is shown in panel 7 of Figure 1. While the SDA predicted that there may be some confusion between the pixels of the background and of the large beads, this confusion evidently occurs at the edge of the beads and thus is difficult to detect in the labeled image. Although not predicted by the SDA, there is evidently

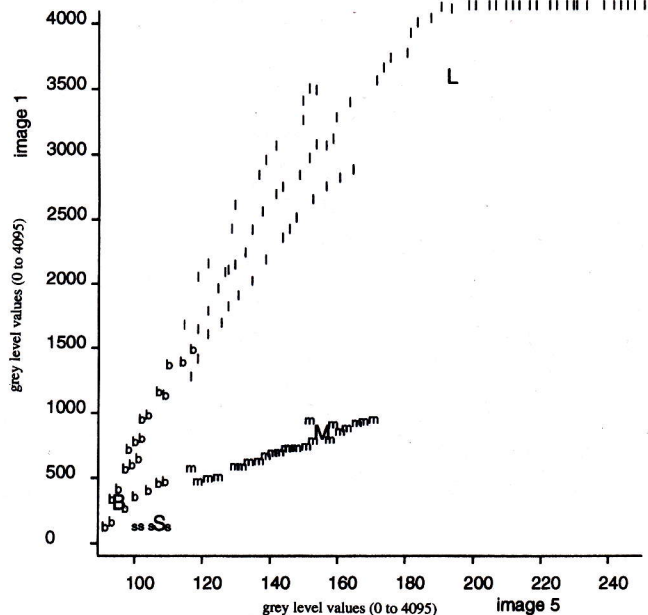


Figure 3. Biplot of the gray level values (0–4095) of the representative learning pixel sets for each bead type and the background in panels 1 and 5 in Figure 1 of the multichannel image: L, large bead; M, medium bead; S, small bead; b, background. The large capital letters indicate the average pixel value for each group.

some small confusion between the pixels of the large beads and the medium beads (since a very small percentage of the two right-hand large beads are incorrectly classified as pixels of the medium beads). In order to verify the quality of the labeling in quantitative terms, the SDA discriminant template created in the learning stage above was applied to 10 “unknown” multichannel images of the beads. The diameters of 50 beads in each size category were

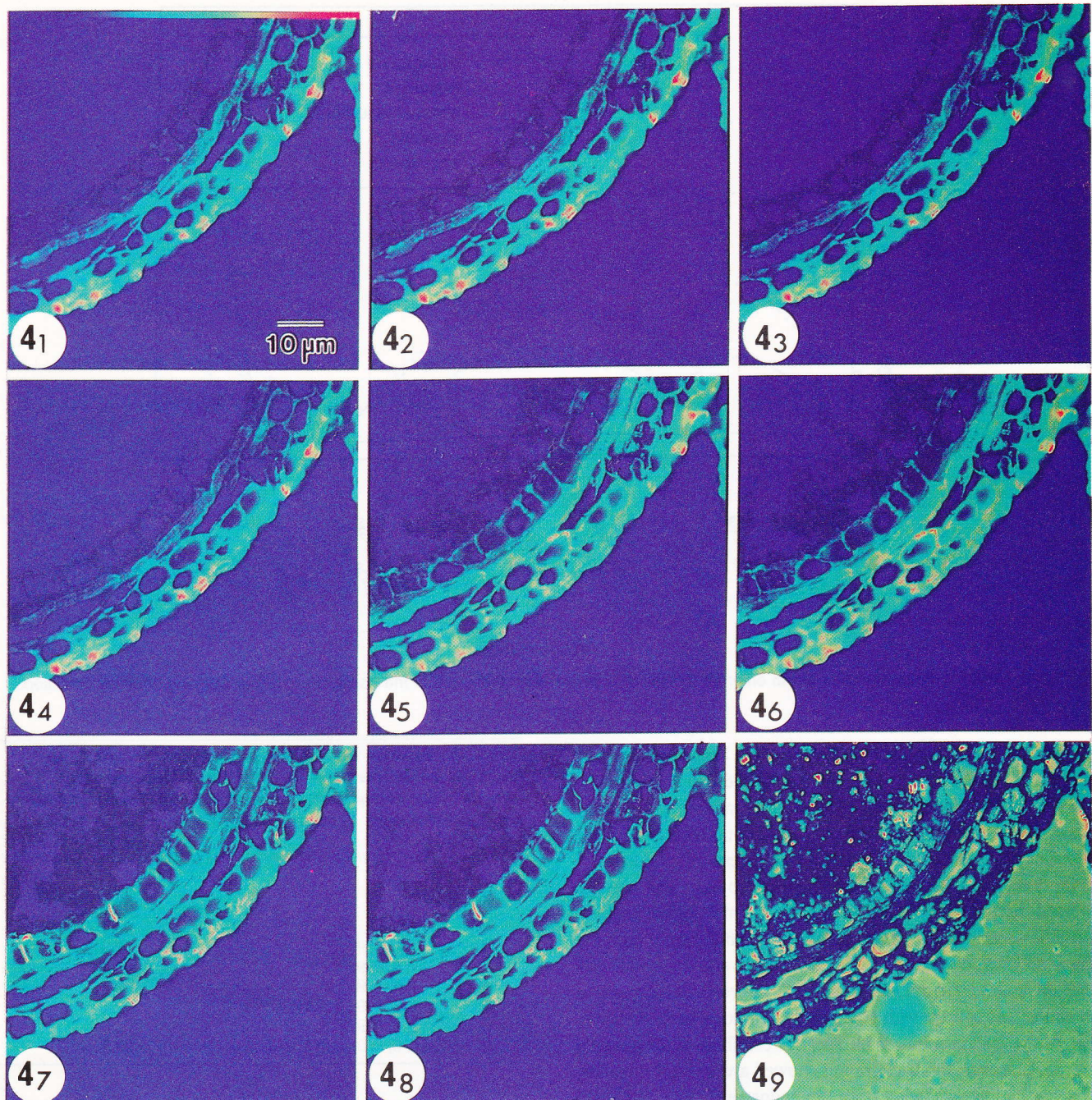


Figure 4. Sequence of nine fluorescence microscopy images showing the fluorescence emission of the different tissues in a wheat grain section under varying spectral conditions. See Figure 5 for details of the spectral conditions.

then measured both in the labeled images and in corresponding bright-field photographs of the beads. Thus, the average real size of the large, medium and small beads were respectively measured to be 15.59 ± 1.00 , 10.80 ± 0.42 , and $3.94 \pm 0.89 \mu\text{m}$. The average labeled bead size for these beads were 16.52 ± 0.57 , 11.23 ± 0.43 , and $4.83 \pm 0.77 \mu\text{m}$, respectively. Consequently, the average percentage differences between the real bead size and the labeled bead size were +5.6, +3.8, and +18.4%, respectively. It is evident that, except for the small beads, the labeled area of the beads corresponds very well with their real size. On average, the size of the beads in the labeled image is slightly overestimated but is still correct with a confidence limit of 94.4% for the large beads, 96.2% for the medium beads, and 81.6% for the small beads. While the error in labeled size of the small bead appears to be more significant than that of the larger beads, the error predominantly

resulted from the greater measurement error involved in measuring small objects.

Thus, in respect of the very high quality of the labeling and discrimination of the four different components in this artificial sample, it is evident that the discriminant analysis method is capable of producing satisfactory labeling of multicomponent samples.

Natural Samples. Wheat Grain Sections and Milled Flours. Sections of wheat grains were studied by epifluorescence microscopy and discriminant analysis in order to test the procedure with more realistic multicomponent samples. Reference schematic diagrams of wheat grain histological organisation are available elsewhere;⁴⁰ however, four main tissues are evident in

(40) Gassner, G. *Mikroskopische Untersuchung pflanzlicher Lebensmittel*; Gustav Fisher Verlag: Stuttgart, Germany, 1973.

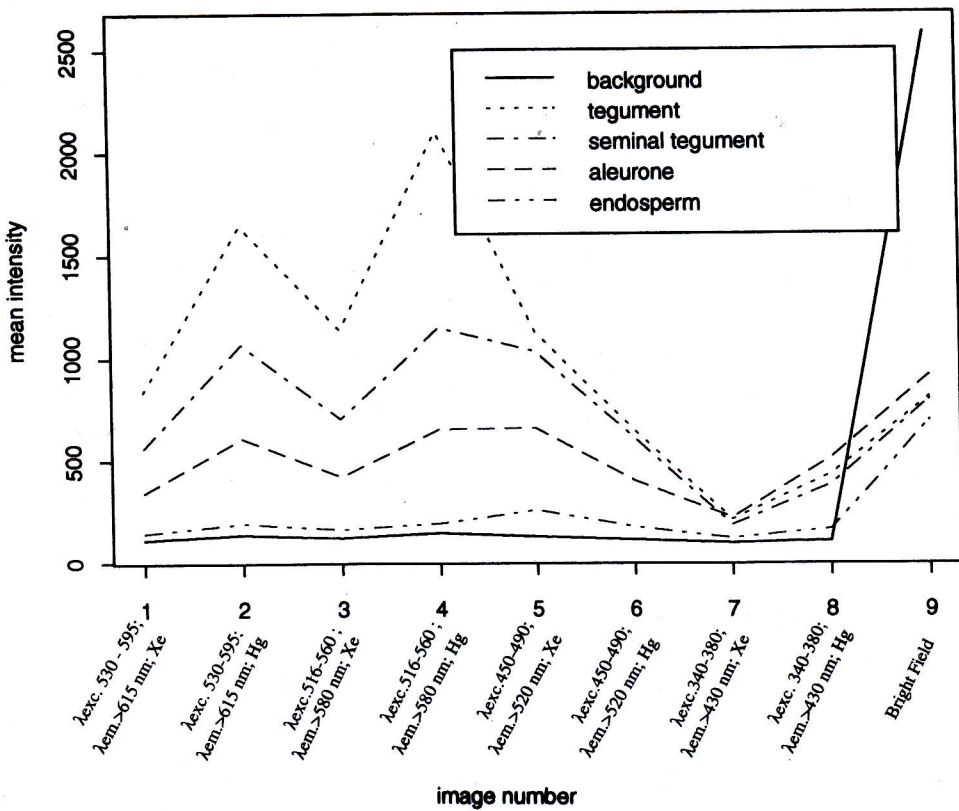


Figure 5. Spectral characteristics of the different tissues in a wheat grain section and the background under the nine spectral conditions.

the starchy region of the grain (namely, the tegument, seminal tegument, aleurone, and endosperm) in addition to the background. A sequence of nine images of the wheat grain sample was acquired under nine different spectral conditions (Figure 4). A total of 200 representative learning pixels were selected for each of the four tissue types and for the background. The average spectral characteristics of the tissues are shown in Figure 5, where it can be seen that the groups presented a difference in both the shape and intensity of their spectra. Under spectral conditions 1–8, the endosperm did not significantly fluoresce and presented an almost flat spectra with low gray level values, very similar to that of the background. With spectral condition 9 (bright-field image), however, the background showed a very high intensity, allowing its discrimination from the endosperm. The tegument and seminal tegument presented strong fluorescence under the first six spectral conditions. The aleurone gave an intermediate fluorescence intensity but was the most fluorescent tissue under UV excitation conditions (panels 7 and 8). SDA was applied in order to select the most discriminant images, as shown in Table 2. The best classification of the learning pixels was achieved using five of the nine images, whereby 990 out of 1000 pixels (i.e., 99.0%) were correctly classified. The 1.0% of misclassified pixels predominantly involved confusion between the aleurone and the seminal tegument, although there was also a small amount of error between the tegument and seminal tegument. The first two selected spectral conditions ($\lambda_{\text{exc}} 530\text{--}595 \text{ nm}$, $\lambda_{\text{em}} > 615 \text{ nm}$, Xe lamp; and $\lambda_{\text{exc}} 450\text{--}490 \text{ nm}$, $\lambda_{\text{em}} > 520 \text{ nm}$, Hg lamp) allowed 94.2% of the learning pixels to be correctly classified, and the corresponding biplot is shown in Figure 6. The groups are generally well separated. It can also be seen that the tegument appears to consist of two subgroups. It is well-known that the tegument is not homogeneous and is actually formed from several different

Table 2. Effects on the Classification Result of the Stepwise Introduction of the Nine Fluorescence Microscopy Images of the Wheat Grain Section into the Discriminant Analysis Algorithm

step no.	no. of images included	% of correctly classified pixels
1	1	86.0
2	1; 6	94.2
3	1; 6; 8	98.4
4	1; 6; 8; 9	98.7
5	1; 6; 8; 9; 7	99.0
6	1; 6; 8; 9; 7; 5	98.4
7	1; 6; 8; 9; 7; 5; 2	97.4
8	1; 6; 8; 9; 7; 5; 2; 3	97.5
9	1; 6; 8; 9; 7; 5; 2; 3; 4	98.3

layers of different cell types, and thus it would appear that SDA is capable of a more detailed discrimination of the cell wall materials in wheat samples than was attempted in the current study. The labeled image produced from the classification is shown in panel 8 of Figure 1. This image is in accordance with published schematic diagrams of wheat grain histology,⁴⁰ and it is therefore visually evident that a good quality of image labeling has been achieved. In addition to the slight misclassification expected from the SDA, there is also, however, some misidentification of the tegument with the endosperm at the periphery of the section. In general, however, the tissue labeling seemed acceptable and compares favorably with the type of results obtained when specific colorations are used (see ref 1 for examples).

The discriminant "template" created by the supervised discriminant analysis of the wheat grain section was then applied to "unknown" multichannel images of the same sample. An example of the resulting labeled images is shown in panel 9 of Figure 1.

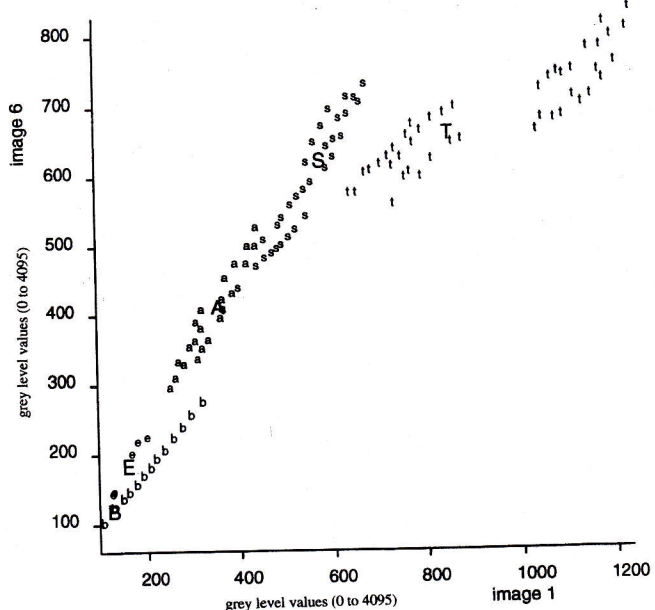


Figure 6. Biplot of the gray level values (0–4095) of the representative learning pixel sets for each tissue in the wheat grain section and for the background in panels 1 and 6 of Figure 4 of the multichannel image: t, tegument; s, seminal tegument; a, aleurone; e, endosperm; b, background. The large capital letters indicate the average pixel value for each group.

The labeling of "unknown" images generally allowed the various tissue types and the background to be distinguished from one another, although in all cases the quality of labeling was inferior to that in the learning image. For example, in panel 9, where the tegument was partially detached from the bulk of the tissue, there was considerably more confusion between the endosperm, the tegument, and the seminal tegument than in the learning image, although it is evident that the endosperm, aleurone, and background are still well labeled.

DISCUSSION

In general, the discrimination between tissues in the learning and "unknown" labeled images was of a high quality (i.e., correct classification and correct labeled object size), particularly for the artificial samples where each component was of a reasonably uniform size and had a distinctly different fluorescence behavior. The generation of labeled images of multicomponent samples represents, for several reasons, a significant advance over conventional microscopic discrimination of different tissues.

First, the labeled digital image of the sample carries clear and discrete information regarding the composition and spatial distribution of the sample. Each component (including the background) is represented by a single gray level value (which is given an arbitrary false color), thus significantly facilitating most standard image analysis techniques due to the ease with which thresholds can be set. For example, quantitative values of the percentage of each component in the sample can be routinely extracted from the histogram of the labeled image. Thus the identity, location, distribution, size, and quantification of the various components in numerous complex, multicomponents samples can be quickly measured. While the percentage quantification of each component does not have a direct relation to the concentration of the fluorochrome present in the sample, the quantification of sample components can be performed without

the need for expensive fluorescence standards and could be useful in applications such as determining the percentage of flour contamination by cell wall materials.

Second, the SDA procedure for identifying different tissues in a complex sample is rapid and greatly decreases the need for operator experience. This is because the learning process (i.e., selection of the representative pixels) only needs to be performed once by an experienced operator, following which the technique can be used by nonexperts. Selection of the learning pixels and the initial creation of the discriminant template requires about 30 min to 1 h, depending on the complexity of the sample, following which the manual acquisition of a nine-image sequence takes ~1 min, with subsequent image labeling requiring ~15 s. Automation of the system using a motorized microscope stage and dedicated software, in which the learning process has previously been performed for various sample sets, could substantially speed up the process, thus facilitating the high number of images required to ensure representativity in any microscopic study.

While a good quality of labeling was evident in the learning image of the natural sample, a deterioration in the quality of the labeling in subsequent "unknown" labeled images was observed. This serves, however, to highlight several important factors involved in determining the quality of "unknown" image labeling. First, the choice of the learning pixels has a significant influence on the quality of the labeling. In this study, we chose 1000 representative pixels for the learning pixel sets. Selection of this number of pixels took ~30 min; however, 1000 pixels represents only 0.04% of the total number of pixels in the image. Increasing the number of pixels selected should increase labeling quality by increasing the representativity of the learning pixel sets, although the time required for the learning stage will be increased. Nevertheless, even with an increased number of pixels in the learning set, there will always be pixels whose spectral signature is ambiguous between two groups (particularly for pixels located at the interface between two components such as the background close to a fluorescent bead). The selection of appropriate spectral conditions for each sample type is therefore highly important in ensuring good discrimination between the components. It may therefore be of interest to develop the possibility of combining a range of spectral conditions (autofluorescence, induced fluorescence via fluorophores, three-channel color vision, near-infrared spectral imaging, etc.). This study also highlights the observation that in the current procedure the discriminant analysis is based on the average fluorescence intensity of the sets of representative pixels. "Unknown" pixels are then attributed to the group that gives the shortest Mahalanobis distance. This, in theory, gives some robustness with respect to the actual intensity of the pixel, and such an effect is evidenced by the good quality of image labeling achieved with the beads, since the beads in each size category, although not exactly identical, had similar diameters (sample thickness) and fluorophore concentrations. It is evident, however, that in a more realistic sample (e.g., cereal sections) the emitted fluorescence intensity can vary greatly even in the same tissue type (due to changing fluorophore concentration, sample thickness/orientation, environment, etc.) and thus a discriminant analysis method based entirely on fluorescence intensity alone is prone to confusion between qualitative groups. For these reasons, we are currently investigating methods to improve the robustness of the technique, including nonintensity-based classification, an improved learning procedure, nearest-

neighbor analysis, consideration of object shape, and a nonsupervised clustering approach to increase the number of pixels in the learning set.

CONCLUSION

The current study demonstrates the application of stepwise discriminant analysis to multichannel fluorescence microscopy images. A high quality of image labeling was achieved, indicating that chemometric labeling of multichannel imaging via SDA is a promising technique for the characterization and testing of

complex samples. Current work is aimed at improving the technique in order to achieve a robust, rapid imaging system for application in quality control systems.

Received for review February 5, 1997. Accepted August 6, 1997.⁸

AC970145X

* Abstract published in *Advance ACS Abstracts*, September 15, 1997.